Direct and inverse pumping in flows with homogeneous and non-homogeneous swirl

A. Pothérat[1], F. Rubiconi[1], Y. Charles[2] and V. Dousset[1*]
[1] *Coventry University, Applied Mathematics Research Centre, priory street Coventry CV1 5FB, UK and*
[2] *Grenoble High Magnetic Field Laboratory and CRETA laboratory/CNRS-Grenoble, France*
(Dated: September 24, 2013)

The conditions in which meridional recirculations appear in swirling flows above a fixed wall are analysed. In the classical Bodewädt problem, where the swirl tends towards an asymptotic value away from the wall, the well-known
"tea-cup effect" drives a flow away from the plate at the centre of the vortex. Simple dimensional arguments applied to a single vortex show that if the intensity of the swirl decreases away from the wall, the sense of the recirculation can be inverted, and that the associated flow rate scales with the swirl gradient. If the flow is quasi-2D, the classical tea-cup effect takes place. This basic theory is confirmed by numerical simulations of a square array of steady, electrically driven vortices. Experiments in the turbulent regimes of the same configuration reveal that these mechanisms are active in the average flow and in its fluctuating part. These mechanisms provide an explanation for previously observed phenomena in electrolyte flows. They also put forward a possible mechanism for the generation of helicity in flows close to two-dimensionality, which plays a key role in the transition between 2D and 3D turbulence.

PACS numbers: 47.32.-y Vortex dynamics, rotating fluids
47.27.nd Turbulence: Channel flow
47.65.-d Magnetohydrodynamics and electrohydrodynamics

INTRODUCTION

The teacup effect is one of the mechanisms actively mixing sugar in a cup of tea when stirring it with a spoon. Under the effect of rotation, a centripetal pressure gradient builds up in the fluid to oppose the centrifugal force. In the boundary layer near the bottom of the cup, the flow is slow so the centrifugal force collapses and the same pressure gradient drives a convergent flow towards the centre of the cup. This feeds the meridional recirculation that is actually responsible for mixing (this configuration is that of the Bodewädt problem). The configuration where a solid wall rotates under a still fluid (Ekman problem) leads to a reversed meridional flow for the same reasons [1, 2].

This type of mechanism is at play in a number of less anecdotal processes, both industrial and natural, such as the stirring of liquid metals (in the Bridgeman process to grow silicone crystals for example [3]) or the generation of cyclones, where it controls the redistribution of momentum, heat or chemicals in the flow. It is particularly important in experiments aiming to reproduce 2D turbulence or to understand the transition between 2D and 3D turbulence [4, 5]: the authors of Refs. [6, 7] recently discovered that the appearance of a third velocity component played a role in the break-down of the inverse energy cascade of 2D turbulence, and was therefore central to understanding this transition. Recent numerical simulations [8] were able to link the existence of the inverse cascade to the presence of helicity even in 3D turbulence. Since the teacup effect is precisely a source of helicity linked to the presence of a bottom wall, it most likely plays an important role in the transition between 2D and 3D turbulence dynamics. The authors of Ref. [9] attempted to suppress it by inserting a "buffer" fluid layer between the container wall and the layer of fluid where turbulence was forced, only to discover that secondary flows still subsisted. Their presence was attributed to confinement itself but also to the non-homogeneity of the forcing, which consisted of passing an electric current through the fluid layer (a conductive electrolyte), placed over an array of magnets of alternate polarity. The nature of these recirculations was not the focus of this particular paper but it can be seen from their results that pumping in this configuration was inverse, with the fluid diving to the centre of vortices in the core of the flow, whereas in homogeneously forced flows between two planes, direct pumping is expected as in the teacup effect [10]. Thus, although the teacup effect is well understood, the conditions in which secondary flows appear and simply which way they flow is not yet clear.

In this paper, we put forward a mechanism to explain how either direct or inverse pumping arises, depending on the homogeneity of the forcing. This scenario is tested against numerical simulations and experiments on a flow of liquid metal between two parallel planes distant of H, subject to a transverse magnetic field $B\mathbf{e}_z$ and where the flow is driven by injecting electric current at one of the walls. This setup offers a convenient way to control the homogeneity of the forcing, because for strong magnetic fields, the Lorentz force diffuses momentum across the fluid layer [11]. When inertia is present, it opposes this effect and diffusion is only achieved over a finite length $l_z \sim l_\perp N^{1/2}$, where the interaction parameter $N = \sigma B^2 l_\perp/(\rho U)$ represents the ratio of the Lorentz force to inertia ($l_\perp$, U, ρ and σ are the the size of the

swirling structure across $\mathbf{B}$, its azimuthal velocity, the density and electric conductivity of the fluid). For high magnetic fields $l_z/H >> 1$ and so momentum diffusion across the channel is effective enough to make the flow quasi-2D. If, on the other hand , $l_z/H < 1$ or $l_z/H \sim 1$, then inertia and momentum diffusion are of the same order and 3D velocity variations are present [12].

GOVERNING EQUATIONS

The velocity and pressure fields $\mathbf{u}$ and p of an incompressible flow of a fluid of density ρ, viscosity ν are governed by the Navier-Stokes and continuity equations:

$$(\partial_t + \mathbf{u}\cdot\nabla)\mathbf{u} + \frac{1}{\rho}\nabla p = \nu\nabla^2\mathbf{u} + \mathbf{f}, \quad (1)$$

$$\nabla\cdot\mathbf{u} = 0. \quad (2)$$

To illustrate the phenomena of direct and inverse pumping, we shall rely on the example of electrically forced flows. The principle is to apply an externally generated, homogeneous magnetic field $B\mathbf{e}_z$ to an electrically conducting fluid and to inject electric current in one or several points of an otherwise electrically insulating wall orthogonal to $\mathbf{e}_z$ (here at $z = 0$). At each such electrode, the Lorentz force creates a vortex spinning around $\mathbf{e}_z$ that extends all the further in the core as B is high [12, 13]. Assuming the magnetic Reynolds number $Rm = \mu\sigma UL$ remains small (U, L are typical velocities and length and μ is the magnetic permeability of vacuum.), then the magnetic field associated to the current $\mathbf{J}$ within the fluid is negligible compared to B, and the Lorentz force to which the flow is subjected expresses as $\mathbf{f} = B\rho^{-1}\mathbf{J}\times\mathbf{e}_z$ [14]. $\mathbf{J}$ is coupled to $\mathbf{u}$ through Ohm's law and charge conservation:

$$\mathbf{J} = \sigma(-\nabla\phi + B\mathbf{u}\times\mathbf{e}_z), \quad (3)$$

$$\nabla\cdot\mathbf{J} = 0, \quad (4)$$

where ϕ is the electric potential. The generic geometry is that of a channel with no-slip, impermeable and electrically insulating walls located at $z = 0$ and $z = H$. The flow is governed by two non-dimensional parameters: the Hartmann number $Ha = BH\sqrt{\sigma/(\rho\nu)}$ and the Reynolds number $Re^0 = \Gamma/\nu$. $\Gamma = I/(2\pi\sqrt{\sigma\rho\nu})$ is the circulation that would be induced around an electrode, in the plane just outside the Hartmann boundary layer at $z = 0$, by injecting a DC current of intensity I through it, if no viscous dissipation was present [12, 13]. Ha^2 represents the ratio of Lorentz to viscous forces but Ha and Re^0 can be thought of as non-dimensional measures of B and I respectively. Thus, Ha controls the momentum diffusion along $\mathbf{B}$ and so decreasing it incurs steeper velocity gradients along $\mathbf{e}_z$ in the core of the flow, and increases the inhomogeneity of the swirl.

NUMERICAL SYSTEM

In the numerical simulations, the fluid is confined in a rectangular box of size $L^2 \times H$ with $L = 0.06$ m and $H = 0.1$ m. The working fluid is GaInSn, an eutectic alloy of Gallium Indium and Tin, of conductivity $\sigma = 3.6\times10^6\ \Omega^{-1}.\mathrm{m}^{-1}$, viscosity $\nu = 4\times10^{-7}\ \mathrm{m}^2.\mathrm{s}^{-1}$ and density $\rho = 6.4\times10^3\ \mathrm{kg.m}^{-3}$. The container is placed in a uniform magnetic field $B\mathbf{e}_z$ so that besides the two Hartmann walls orthogonal to it, there are also four walls parallel to it. All walls are impermeable, no slip and electrically insulating. The flow is driven by injecting a DC current of alternate polarity through a square array of 6 $\times$ 6 electrodes of diameter 1 mm, mounted flush at the bottom wall, spaced by distance $L_i = 0.01$ cm.

The code is based on the finite volumes method implemented in the OpenFOAM framework and solves the three-dimensional, time-dependent equations in a segregated way. The numerical scheme is the consistent and conservative algorithm put forward in Ref. [15]. The code is described and fully tested in the more complex configuration of the flow around a 3D obstacle in Ref. [16]. To summarise it, the spatial discretisation is of second order, the time-scheme is a second order implicit pressure-velocity formulation and the pressure-velocity coupling is solved with the PISO algorithm implemented as in Ref. [17]. The time step is chosen so that the maximum Courant number $C = U\Delta t/\Delta x$ is well below 1 and the maximum of $D = \nu\Delta t/\Delta x^2$ remains below 10 (Courant-Friedrich-Lewy conditions). Collocated and structured meshes made of 1 917 971 and 4 227 768 rectangular elements are respectively used for simulations at $Ha = 800$ and $Ha = 1822$. In order to keep the mesh orthogonal, the electrodes, which are circular in the experiment, are modelled by squares of size 1 mm. The mesh is regular outside of the boundary layers and refined near the walls so as to always keep 4 points across the Hartmann layers and 3 points across the Shercliff layers.

For each value of Ha, the flow is initially at rest and the lowest current is injected. In all computations presented here, the flow stabilised into a steady state, which was used as initial condition for the simulation at the same Ha, for the next value of Re^0 up.

MECHANISMS OF INVERSE AND DIRECT PUMPING

We shall first illustrate the basic mechanism of inverse pumping on the example of a steady flow in the configuration described in the previous section. Figure 1 shows the pressure contours and streamlines obtained at $Ha = 1.822\times10^3$ and $Re^0 = 171$. These are typical of the flow patterns obtained for other parameters. The flow consists of a square lattice of 6×6 vortices rotating

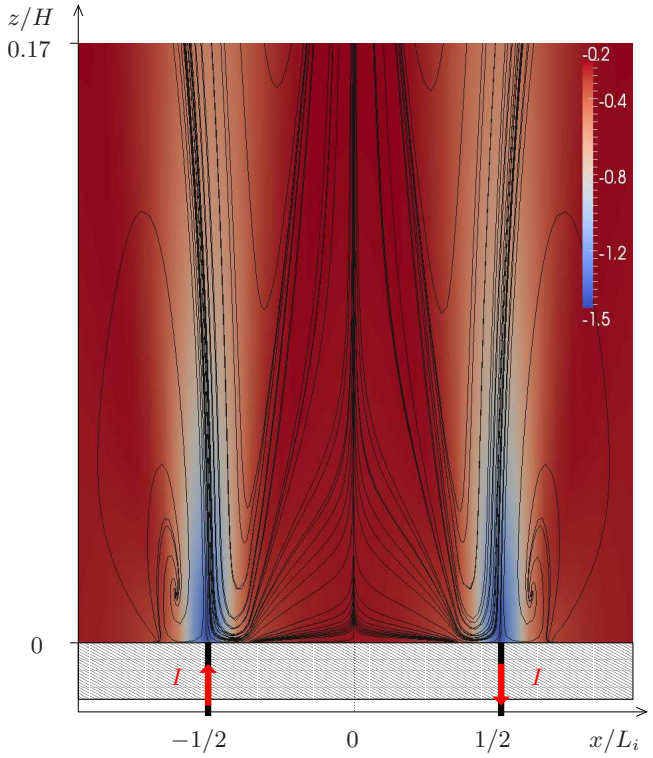

FIG. 1. Streamlines of (u_x, u_z) in the plane $y = L_i/2$, intercepting the axis of rotation of two vortices and contours of pressure (colours). Pressure is normalised by ρu_M^2 where $u_M = \max\{u_y(x,z)\}$ is the maximum azimuthal velocity within any given vortex in the vessel. Downward vertical jets occur right in the region of lowest pressure at the centre of vortices at $x = \pm L_i/2$. The fluid domain extends over $(x/L_i, y/L_i, z/H) \in [-3,3]^2 \times [0,1]$, but only the region $[-1,1] \times \{1/2\} \times [0, 0.17]$ is represented here.

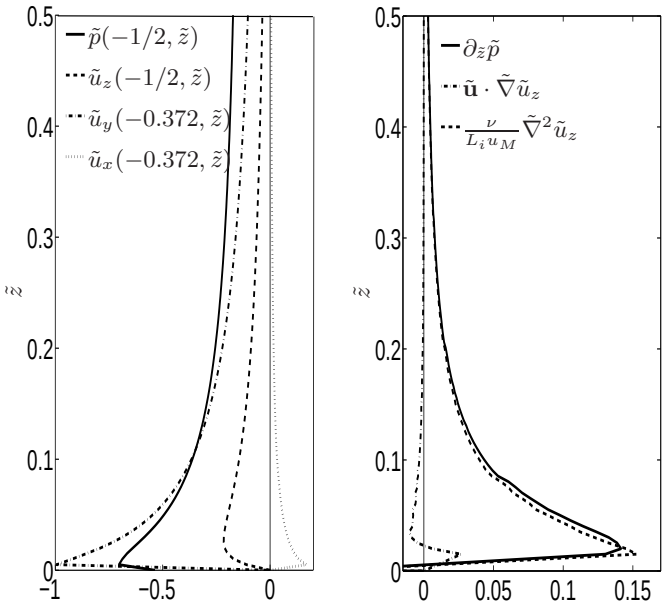

FIG. 2. Left: profiles of pressure and velocity in the plane $y/L_i = 1/2$, along the columnar vortex centred at $(x/L_i, y/L_i) = (-1/2, 1/2)$. Right: variations of the different terms in $(1)\cdot\mathbf{e}_z$ along the axis of rotation of the same vortex. The vertical pressure gradient balances lateral viscous friction to a good approximation in the core. Velocities, pressure, horizontal and z coordinates marked $\tilde{q}$ were respectively normalised by $u_M = \max\{u_y(x,z)\}$, ρu_M^2, L_i and H.

along $\mathbf{e}_z$ with alternate spin. A strong downward flow exists at the centre of each of them that loops back up in the outer part of the vortices. To illustrate the underlying mechanism, we shall reason on a single vortex of radius $l_\perp$, with associated polar coordinates centred on it ($r^2 = (x + L_i/2)^2 + (y - L_i/2)^2$, and the radial and azimuthal velocity in this vortex respectively correspond to u_x and u_y in the plane $y = L_i/2$, on figure 1). The pressure contours in figure 1 and vertical profiles of p and u_z (figure 2, left) show that the downward jet coincides with a strong pressure gradient. Plots of the different terms in $(1)\cdot\mathbf{e}_z$ (figure 2 , right) show that the latter is only opposed by viscous friction:

$$\partial_z p \sim -\rho\nu \frac{u_z}{l_\perp^2}. \tag{5}$$

The pressure drop at the centre of the vortex results from the centripetal pressure gradient that opposes the centrifugal force:

$$p(r=0,z) - p(r=l_\perp,z) \sim -\rho u_\theta^2(r=l_\perp,z). \tag{6}$$

Contours of p on figure 1 suggest that the pressure gradient outside of the vortex $\partial_z p(l_\perp, z)$ is negligible. The maximum u_z^M of $u_z(0,z)$ is located at $z = z_0$, near the bottom wall, but still outside the boundary layer (see figure 2, left) and can be estimated from (5) and (6):

$$\frac{u_z(0,z_0)}{u_\theta(l_\perp,z_0)} \sim Re^\nabla, \tag{7}$$

where $Re^\nabla = 2\partial_z u_\theta(l_\perp,z_0) l_\perp^2/\nu$ is a Reynolds number built on the vertical gradient of the swirl. Eq. (7) expresses that vertical motion is driven by the inhomogeneity of the swirl. Mass conservation requires that the flow impacting the wall must turn radially:

$$u_r(z_0) \sim -\frac{l_\perp}{2h^r} u_z(0,z_0) \sim -u_\theta^o \frac{l_\perp}{2h^r} Re^\nabla, \tag{8}$$

where, $u_\theta^o = u_\theta(l_\perp, z_0)$, h^r is the height over which the return flow takes place, typically of the same order as $l_\perp$ in all simulations.

Unlike inverse pumping, direct pumping is driven in the wall boundary layer by the radial pressure gradient that builds up in the core to oppose the centrifugal force (6). If δ is the boundary layer thickness, $(1)\cdot\mathbf{e}_z$ implies that the pressure cannot vary across it and so the radial pressure gradient there is the same as in the core. Since u_θ

becomes small in the boundary layer, so does the centrifugal force $\rho u_\theta^2/r$. Hence, (1)$\cdot\mathbf{e}_r$ there expresses that in the boundary layer, the centripetal pressure gradient is balanced by viscous friction. If inverse pumping is present, however, the associated radial flow in the core, expressed by (8), considerably enhances radial friction $\nu\partial_{zz}^2 u_r$ in the boundary layer. Denoting quantities within the boundary layer with a superscript b, it comes that

$$\partial_r p^b \sim -\frac{\rho\nu}{\delta^2}(u_r^b - u_r(z_0)), \tag{9}$$

and from (6) and (8),

$$\frac{u_r^b}{u_\theta^o} \sim -\frac{l_\perp}{2h^r} Re^\nabla - \left(\frac{\delta}{l_\perp}\right)^2 Re, \tag{10}$$

where, unlike Re^0, the Reynolds number $Re = u_\theta^o l_\perp/\nu$ is based on u_θ^o, a measured quantity. For direct pumping to exist, the flow must be directed radially inwards within the boundary layer. When $\partial_z u_\theta < 0$, as in the case studied here, this imposes the condition:

$$|\partial_z u_\theta| < \left(\frac{\delta}{l_\perp}\right)^2 \frac{h^r}{l_\perp}\left|\frac{u_\theta^o}{l_\perp}\right|. \tag{11}$$

In all numerical simulations, h^r was typically of the order of $l_\perp$. Boundary layers are thin, so $l_\perp/\delta >> 1$ (in electrically driven flows, the wall boundary layer is a Hartmann layer, with thickness $\delta/H = Ha^{-1}$, so $l_\perp/\delta \sim Ha$). Since the flow is quasi-2D as soon as $\partial_z \mathbf{u} = \mathcal{O}(\delta/l_\perp)$ outside the boundary layer, rather than an exact criterion on $|\partial_z u_\theta|$ for the appearance of inverse pumping, (11) mainly expresses that inverse pumping can only exist when the swirl is quasi-2D. This result explains why direct pumping was never observed in any of our simulations: in all numerically accessible regimes, the inhomogeneity of the swirl was always sufficient to drive inverse pumping. Similarly, in the wall-bounded electrolytes layers studied by Ref. [18], vortices were driven by imposing an electric current in the field created by permanent magnets placed underneath the layer. The swirl inhomogeneity resulted directly from that of the magnetic field and so $\partial_z u_\theta$ and u_θ/H were of the same order, making it impossible for (11) to be satisfied. It is therefore not surprising that inverse pumping was observed in this case too.

In quasi-2D flows, by contrast, $Re^\nabla \simeq 0$ and from (10) and (2), direct pumping drives a flow from the boundary layer into the core:

$$\frac{u_z}{u_\theta^o} \sim 2\left(\frac{\delta}{l_\perp}\right)^3 Re. \tag{12}$$

In electrically driven flows, $\delta = H/Ha$ and scaling (12) coincides with the expression derived by Ref. [19] from matched asymptotics. Ref.[13] provides a clear example of direct pumping in a large electrically driven vortex confined in a cylindrical vessel of diameter 12 cm filled with a layer of mercury of thickness $H = 1.92$ cm, placed in axial homogeneous magnetic field of 0. In these conditions, the ratio of magnetic diffusion length l_z to H was much larger than unity (typically between 10^2 and 6×10^2) and so the flow was indeed quasi-2D, as required by condition (11). The numerical simulations of Ref.[20] together with the measurements of radial profiles of azimuthal velocity confirmed that direct pumping in this case scaled as (12).

We shall conclude this theoretical section with two more remarks: firstly, it should be noticed that should the swirl be inhomogeneous in such a way that $\partial_z|u_\theta| > 0$, then direct pumping would occur, but u_z would still scale as in (7). Secondly, (11) provides a criterion for the existence of direct Bodewädt pumping, not a criterion for the disappearance of inverse pumping. In theory, one could imagine a flow that would be quasi-2D to a precision of $\mathcal{O}(\delta/H)^2$ and therefore with direct pumping, but with a residual three-dimensionality of higher order, which would suffice to drive a faint inverse pumping at the same time. More realistically, $|\partial_z u_\theta|$ may vary along $\mathbf{e}_z$, in such a way that it can satisfy (11) in the vicinity of at least one of the walls but not everywhere. The corresponding secondary flow could then feature a complex succession of recirculations in any direction. One such example shall be found in turbulent flows (section).

INVERSE PUMPING IN THE SQUARE VORTEX ARRAY

Numerical simulations of the vortex array present specific features that differ from those of an isolated vortex, on which the theory is based. Despite this difference, figure 3 shows that the vertical velocity $u_z(z_0)$ within a single vortex in the array linearly increases with Re^∇. Scaling (7), is thus still satisfied, albeit with a reasonable amount of data scattering. This scattering can be partly attributed to the plotted values being local ones, and partly to interaction between vortices. Most importantly, data obtained for different values of Ha collapse on the same line, which confirms Re^∇ as the single relevant parameter for inverse pumping. This stresses that it is the gradient of swirl that determines inverse pumping, not how this gradient is generated, electromagnetically or in any other way. Furthermore, all simulated cases involve strongly inhomogeneous swirl, with $\partial_z|u_\theta| \gtrsim |u_\theta|/H$ and exhibit inverse pumping, and no direct pumping, in agreement with condition (11) too.

Unlike when isolated, vortices embedded in an array undergo a strong influence from neighbouring vortices. In an infinitely extended square array, this would mainly translate into a loss of axisymmetry of individual vortices, with streamlines progressively deforming to a square shape, away from the vortex cores. In our numerical simulations, by contrast, the 6×6 array is bounded by

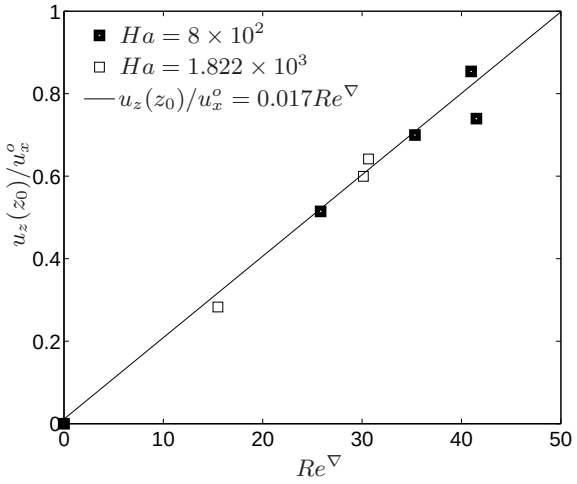

FIG. 3. Scaled maximum vertical velocity vs. Re^∇, from numerical simulations of the 6×6 vortex array in steady state (Re^∇ gives a measure of the gradient of swirl along $\mathbf{e}_z$). Re^∇ was calculated with $l_\perp = L_i/4$.

lateral walls. These incur significant friction on peripheral structures, which are consequently weaker, and less influent than those near the centre. As a consequence, the upper part of the vortex axes is slightly diverted away from the centre, instead of being straight. Nevertheless, as vortices are driven by injecting current from the bottom wall, they remain attached to the electrodes in this region, and the effect of the imbalance between centre and peripheral vortices becomes more visible away from the bottom wall (This can be noticed in figure 1). A second property of vortex arrays is that radial flows induced in neighbouring vortices by inverse pumping collide to form a strong return flow that spirals up in the region between vortices (This pattern is reflected in the vertical jet at $x = 0$ in the streamlines of (u_x, u_z) in figure 1). When Re^0 is increased, these phenomena become more pronounced, and at $Re^0 = 171$ (for $Ha = 800$) and $Re^0 = 512$ (for $Ha = 1822$), recirculations merge in the upper part of the vessel, to the point where they cannot be distinguished from each other anymore.

DIRECT AND INVERSE PUMPING IN TURBULENT FLOWS

We shall now illustrate the occurrence of inverse pumping in more complex flows, such as turbulent flows. Since the corresponding regimes lie beyond the reach of numerical simulations, these shall be analysed experimentally. The experimental setup closely matches the configuration of the numerical simulations with one difference: the dimensions of the vessel across the magnetic field are $L \times L = 0.1\text{m} \times 0.1\text{m}$ instead of $L \times L = 0.06\text{m} \times 0.06\text{m}$. The distance between electrodes where the current is injected can be set to $L_i = 0.01\text{m}$ (as in the numerical simulations) or $L_i = 0.03\text{m}$. A full description of the rig can be found in [12, 21]. Since the influence of the walls becomes more pronounced when L_i/L increases, the numerical simulations present an intermediate case between the two injections scales available in the experiment. For the purpose of this work, the rig was equipped with ultrasound sensor-transducers fitted flush in the top wall and in one of the lateral walls, connected either to a DOP1000 or a DOP3010 ultrasound velocimeter, manufactured by SIGNAL PROCESSING. Ultrasound velocimetry is the method of choice to obtain instantaneous velocity profiles in opaque fluids and is now well developed for liquid metal flows [22, 23]. These probes provide instantaneous profiles of u_z along $\mathbf{e}_z$ at $(x, y) = (-1.5\text{cm}, 1.5\text{cm})$ (probe V1, aligned with a current injection electrode), as well as 5 horizontal profiles of u_x along $\mathbf{e}_x$ at $z \in \{0.12H,\ 0.31H,\ 0.5H,\ 0.69H,\ 0.88H\}$ (probes H1 to H5), also halfway between two electrodes. This gives us access to the variations of horizontal velocity. The signals were reliable up to resolutions of 15Hz and 2mm. In subsequent experiments, a constant current is injected in a fluid initially at rest and all results presented thereafter are obtained when the flow has reached a statistically steady state. The flow is in a turbulent state, where fluctuations exceed the intensity of the average flow.

Figure 4 shows the time-averaged profiles of $u_z(-1.5\text{cm}, 1.5\text{cm}, z)$ obtained from probe V1, and $u_x(0, 0, z)$ from probes H1 to H5, as well as the RMS of the fluctuations of these quantities (respectively denoted as $\langle\cdot\rangle$ and $\langle\cdot'^2\rangle^{1/2}$). For $L_i/H = 0.1$, $Ha = 1.0932 \times 10^4$ and $Re^0 = 2.488 \times 10^4$, the average and the fluctuations of the swirl are clearly 3D, as $|u_x(z)|$ noticeably decreases away from the bottom wall. Inverse pumping is present in the lower half of the vessel, in agreement with the prediction of (11). The general shape of profile $\langle u_z(z)\rangle$ qualitatively follows (7), in the sense that $\langle u_z(z)\rangle$ is more intense where the gradient of swirl is stronger. Furthermore, faint direct pumping can be noticed in the vicinity of the upper plate (with the flow directed away from the plate, see insert in figure 4). This local effect takes place in a region where both the swirl and its vertical gradient are weak. Over a short range of values of z, between the regions of direct and inverse pumping, $u_z(z)$ becomes slightly positive, suggesting that a counter-rotating "connecting" recirculation is present between the co-rotating recirculations associated to direct and inverse pumping. The profile of fluctuations does not provide the direction of the vertical fluctuating flow, but still shows it is strong. Its intensity is stronger in regions of stronger vertical gradients of $\langle u_x(0, 0, z)'^2\rangle^{1/2}$, which suggests that it is also driven by the inverse pumping mechanism.
For $L_i/H = 0.3$, $Ha = 7.288 \times 10^3$ and $Re^0 = 3.11 \times 10^3$, larger, slower vortices are more sensitive to momentum diffusion by the Lorentz force and the flow is correspondingly closer to quasi two-dimensionality. Plots of horizon-

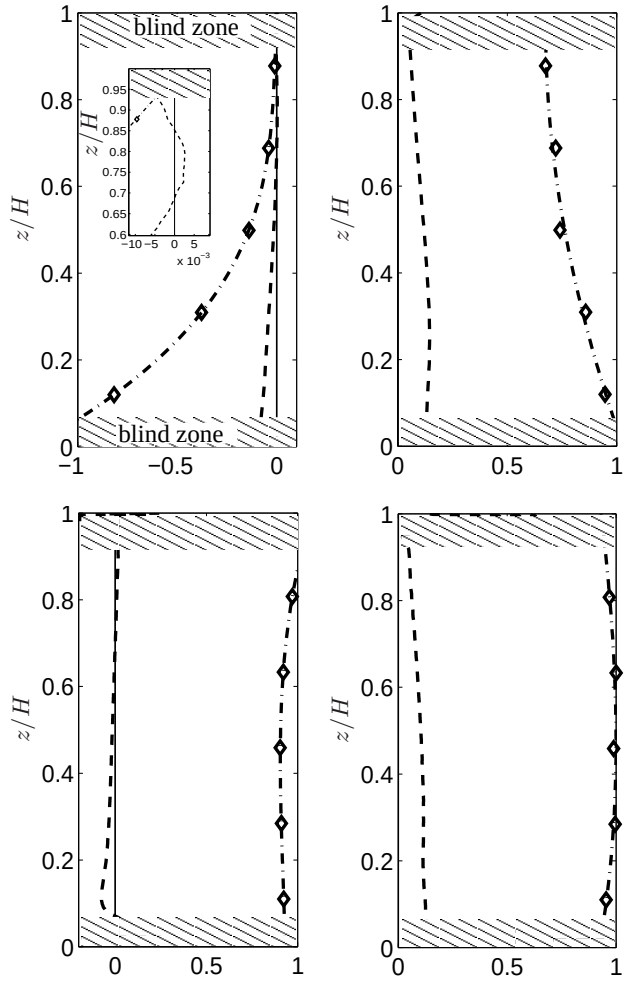

FIG. 4. Profiles of time-averaged horizontal and vertical velocities (left) and RMS of velocity fluctuations (right) obtained by ultrasound velocimetry. Average velocities (resp. fluctuations) are normalised by $\max\{\langle u_x(x,z)\rangle\}$, (resp. $\max\{\langle u_x(x,z)'^2\rangle^{1/2}\}$). Dash: vertical velocity, diamonds: value of u_x (average and fluctuations) measured at $(x/H, y/H, z/H) = (0, 0, z/H)$, dash-dot: order 3 polynomial fit for u_x, top: $Ha = 1.0932 \times 10^4$, $Re^0 = 2.488 \times 10^4$, $L_i/H = 0.1$, bottom: $Ha = 7.288 \times 10^3$, $Re^0 = 3.11 \times 10^3$, $L_i/H = 0.3$. The insert in the upper left graph represents a magnification of the profiles in the vicinity of the upper blind zone, stressing the existence of a small zone where $u_z > 0$.

tal velocity in figure 4 show that the average flow nevertheless still displays the trace of the forcing, with velocities that are highest near the bottom wall, high near the top wall (because of the strong electric current present in the top Hartmann layer) and weaker in the middle, where inertial effects take away energy of the main flow (The mechanisms governing three-dimensionality in wall bounded MHD flows are analysed in detail in [12]). Remarkably, this small three-dimensionality in the horizontal velocity profiles is sufficient to drive inverse pumping in the vicinity of both top an bottom walls and supersede direct Bodewädt pumping, in line with our theoretical prediction that direct pumping can only occur in quasi-2D flows. The profile of $\langle u_x(0,0,z)'^2\rangle^{1/2}$ is practically quadratic and symmetric with respect to $z/H = 1/2$. The maximum intensity of the fluctuations of horizontal velocity corresponds to the minimum of those of the average, from which they draw energy (near $z/H = 1/2$). This phenomenon, called "Barrel effect", was first predicted theoretically [19], then found numerically [24] and was recently shown to act as a general mechanism of appearance of three-dimensionality in wall bounded flows [25]. These measurements constitute the first experimental observation of this effect. The vertical velocity is strongly fluctuating too, but the low value of the gradients of $\langle u_x(0,0,z)'^2\rangle^{1/2}$ does not allow us to conclude as to whether the fluctuations correspond to direct or inverse pumping in this case.

CONCLUSION

Theory, numerical simulations and experiments concur to show that direct recirculations can be inverted (or reinforced) when velocity gradients appear in the third direction. This phenomenon does not only take place in steady vortices but also in fluctuating structures, which raises the question of its relevance to fluctuations at the different scales of turbulent flows. The appearance or the inversion of secondary flows in turbulent structures indeed provide mechanisms to create helicity or to reverse its sign. Since the sense of the energy cascade is tightly linked to signed helicity [8], they could play an important role in the transition between direct and inverse energy cascades. Nevertheless, our early experimental observations of turbulent flows show that inverse pumping combines with other effects to drive complex flow patterns with an helicity that can change sign along the transverse direction in a far from straightforward way.

The authors are indebted to The CRETA and LnCMI CNRS laboratories in Grenoble, and in particular, to Dr. André Sulpice and Dr. François Debray for hosting and supporting the experiment, to Dr. Antoine Alemany (SIMAP-Madylam/CNRS) and Dr. Henri-Claude Nataf (ISTERRE/CNRS) for making their ultrasound velocimeters available to them over extended periods of time.

* alban.potherat@coventry.ac.uk

[1] Ekman, V. W. Ark. Mat., Astron. Fys **2**, 1–52 (1905).
[2] Bödewadt, U. T. Zeitschrift Für Angewandte Mathematik Und Mechanik **20**, 241–253 (1940).
[3] Ammon, L. G., Pedchenko, A., Feodorov, A., Tomzigb,

E., Virbulisb, J., and V., W. J. Cryst. Growth (257), 7–18 (2003).
[4] Paret, J. and Tabeling, P. Phys. Rev. Lett. **79**(21), 4162 (1997).
[5] Sommeria, J. J. Fluid Mech. **170**, 139–168 (1986).
[6] Shats, M., Byrne, D., and Xia, H. Phys. Rev. Lett. **105**, 264501 December (2010).
[7] Xia, H., Byrne, D., Falkovich, G., and Shats, M. Nature Physics **7**, 321–324 (2011).
[8] Biferale, L., Musacchio, S., and Toschi, F. Phys. Rev. Lett. **108**(16), 164501 (2012).
[9] Akkermans, R. A. D., Kamp, L. P. J., Clercx, H. J. H., and Van Heijst, G. H. F. EPL (Europhys. Lett.) **83**(2), 24001 (2008).
[10] Greenspan, H. P. Theory of Rotating Fluids, The. Cambridge University Press, (1969).
[11] Sommeria, J. and Moreau, R. J. Fluid Mech. **118**, 507–518 (1982).
[12] Pothérat, A. and Klein, R. J. Fluid Mech. , submitted, arXiv:1305:7105 (2014).
[13] Sommeria, J. J. Fluid Mech. **189**, 553–569 (1988).
[14] Roberts, P. H. Introduction to Magnetohydrodynamics. Longmans, (1967).
[15] Ni, M. J., Munipalli, R., Morley, N. B., Huang, P. Y., and Abdou, M. J. Comp. Phys. **227**, 174–204 (2007).
[16] Dousset, V. and Pothérat, A. J. Fluid Mech. **691**, 341–367 (2012).
[17] Fureby, H. G. W., Tabor, G., Jasak, H., and C. J. Comp. Phys. **6**(12), 620–631 (1998).
[18] Akkermans, R. A. D., Cieslik, A. R., Kamp, L. P. J., Trieling, R. R., Clercx, H. J. H., and van Heijst, G. J. F. Phys. Fluids **20**, 116601 (2008).
[19] Pothérat, A., Sommeria, J., and Moreau, R. J. Fluid Mech. **424**, 75–100 (2000).
[20] Pothérat, A., Sommeria, J., and Moreau, R. J. Fluid Mech. **534**, 115–143 (2005).
[21] Klein, R. and Pothérat, A. Phys. Rev. Lett. **104**(3), 034502 (2010).
[22] Brito, D., Nataf, H. C., Cardin, P., Aubert, J., and P., M. J. Exp. Fluids **31**(6), 653–663 (2001).
[23] Brito, D., Alboussière, T., Cardin, P., Gagnière, N., Jault, D., La Rizza, P., Masson, J. P., Nataf, H. C., and Schmitt, D. Phys. Rev. E , 066310 (2011).
[24] Mück, B., Günter, C., and Bühler, L. J. Fluid Mech. **418**, 265–295 (2000).
[25] Pothérat, A. EPL (Europhys. Lett.) **98**(6), 64003 (2012).